Chinese Journal of
POLYMER SCIENCE

RESEARCH ARTICLE

https://doi.org/10.1007/s10118-026-3771-x
Chinese J. Polym. Sci.

Synergistic Toughening of Polypropylene Alloys Using Core-Shell High-density Polyethylene/Ethylene-Propylene Rubber and Isoprene Rubber Composite Rubber Particles

Hai-Bo Wang[a], Ang-Xuan Wu[a,b], Jia-Hao Shen[a], Xiao-Tian Nan[a], Feng-Bo Zhu[a], Wen-Wen Yu[a*], and Qiang Zheng[a,c*]

[a] *College of Materials Science and Engineering, Taiyuan University of Technology, Taiyuan 030024, China*
[b] *School of Materials Science and Engineering, Tsinghua University, Beijing 100084, China*
[c] *Department of Polymer Science and Engineering, Zhejiang University, Hangzhou 310027, China*

Electronic Supplementary Information

Abstract Polypropylene (PP) can be toughened by adding elastomers or constructing core-shell structures, although the toughening efficiency of both approaches is limited. Herein, a synergistic dual-phase toughening method is proposed by introducing high-density polyethylene (HDPE) into ethylene-propylene rubber (EPR) and isoprene rubber (IR) composite systems. This resulted in an HDPE@EPR core-shell particle structure alongside finely dispersed IR particles. Interfacial tension promotes adhesion between the EPR shell and IR, concurrently reducing the size of the IR domains and interparticle spacing of the rubber phase. By optimizing the HDPE content, a loading of 15 phr resulted in a well-defined core-shell morphology with minimized IR domains. This enables the fabrication of a PP alloy exhibiting exceptional low-temperature impact toughness (35.8 kJ/m^2 at −20 °C) and an optimal strength-toughness balance. However, surpassing the optimal HDPE content triggers IR particle aggregation, because the thinned EPR shell fails to fully encapsulate the HDPE core, while interfacial tension-driven repulsion facilitates this process. Finite-element simulation results demonstrated a significant synergistic toughening effect between the HDPE@EPR core-shell particles and IR particles. Under low-temperature impact loading, stress and strain are concentrated at the core-shell interface and around the IR particles, which effectively inhibits rapid crack propagation, thereby significantly enhancing the low-temperature toughness of the material. This dual-dispersed phase design strategy offers a promising pathway for the development of high-performance PP composites for demanding low-temperature applications.

Keywords Polypropylene; Core-shell structure; Phase morphology evolution; Synergistic toughening; Finite element simulation

Citation: Wang, H. B.; Wu, A. X.; Shen, J. H.; Nan, X. T.; Zhu, F. B.; Yu, W. W.; Zheng, Q. Synergistic toughening of polypropylene alloys using core-shell high-density polyethylene/ethylene-propylene rubber and isoprene rubber composite rubber particles. *Chinese J. Polym. Sci.* https://doi.org/10.1007/s10118-026-3771-x

INTRODUCTION

Polypropylene (PP) exhibits excellent mechanical properties; however, its impact resistance is poor, particularly at low temperatures. This limitation significantly restricts their widespread application in demanding environments. In recent years, toughening techniques for PP have primarily included physical toughening (*e.g.*, rubber toughening,[1–4] core-shell particle toughening,[5–8] and inorganic filler toughening[9–14]) and chemical toughening (*e.g.*, interfacial capacitance enhancement, vulcanizing agent cross-linking,[2,3,14–16] and IPC for high-impact PP[17]).

It is well known that incorporating rubber into a plastic matrix can enhance the toughness of plastics.[18,19] However, in rubber-toughened plastic systems, it is difficult to simultaneously achieve both high tensile strength and high impact toughness. Several advanced techniques have been developed to achieve a balance between the strength and toughness of PP and PP composites.[11,18,20–27] Among these methods, increasing the rigidity of dispersed phase particles—by adding inorganic or organic rigid particles—has proven to be an effective strategy for obtaining polymeric materials with a balanced combination of strength and toughness. For instance, incorporating core-shell structures[1,8] into rubber-toughened PP. Within this architecture, the rigid core facilitated efficient stress transfer and enhanced the load-bearing capacity, while the soft elastic shell promoted stress dissipation through cavitation and induced shear yielding in the matrix.[28–31] Li *et al.* further found that optimizing the core-shell modulus ratio, specifically by employing a higher core

* Corresponding authors, E-mail: yuwenwen@tyut.edu.cn (W.W.Y.)
E-mail: zhengqiang@tyut.edu.cn (Q.Z.)
Received March 31, 2026; Accepted June 4, 2026; Published online August 28, 2026

modulus and a lower shell modulus, significantly increases the rigidity of polymer composites while maintaining high impact toughness.[30] Shangguan *et al.* demonstrated that a core-shell structure can be created *via* simple melt blending, which effectively increases the interfacial area of the ethylene-propylene rubber (EPR) phase and enhances the equivalent content of the rubber phase in the system, thereby significantly improving the impact performance of the PP alloy.[5,7,8,17,32] However, the toughening effect of a single-rubber system inherently reaches a theoretical upper limit and is often accompanied by challenges such as oversized dispersed-phase particles and non-uniform distribution. Furthermore, achieving a balance between impact strength and stiffness by controlling the dispersed phase size and distribution uniformity using physical method, remains challenging.

Previous studies have demonstrated that composite rubber exhibits superior toughening effects compared to single rubber. For instance, Fowler *et al.* used a styrene-butadiene-styrene block copolymer (SBS) and emulsion-made methyl methacrylate-grafted rubber to toughen the styrene-acrylonitrile copolymer (SAN).[32] The results indicated that even at high concentrations (up to 50%), a single rubber failed to significantly improve the toughness of SAN. In contrast, the hybrid rubber system generated a remarkable synergistic toughening effect, far surpassing the performance of the individual rubbers. This synergy underpins the design of several industrial rubber materials.[33]

Building on this, polymer core-shell particles offer superior toughening effects compared to conventional elastomers, whereas composite rubber systems exhibit synergistic enhancement effects that surpass those of single-rubber systems. Isoprene rubber (IR)[34,35] offers high elasticity, relatively good low-temperature resistance, and high tensile strength, while EPR exhibits excellent compatibility with PP.[36–38] In this study, IR composite rubber particles were introduced based on the traditional core-shell particles formed by high-density polyethylene (HDPE) and EPR (HDPE@EPR) for the purpose of toughening PP. Critically, we exploited the interfacial tension of the HDPE@EPR core-shell particles to simultaneously reduce the size of the composite IR particles through EPR shell-IR adhesion driven by interfacial tension. This process also achieves synergistic toughening between the HDPE@EPR core-shell particles and the IR composite rubber. By adjusting the HDPE core content, we effectively optimized the size distribution of the dispersed phase, thereby successfully preparing a PP alloy that combines excellent low-temperature impact toughness with favorable strength-toughness balance. Through a systematic investigation of the morphology, rheological behavior, and dynamic mechanical properties, combined with finite element simulation analysis, the synergistic toughening mechanism of the HDPE@EPR core-shell particles and IR rubber particles on PP was further elucidated.

MATERIALS AND METHODS

Materials

Commercial grade isotactic polypropylene (*i*PP, T300, melt mass-flow rate (MFR): 3.0 g per 10 min (ISO 1133), M_w=21.0×10^4, M_w/M_n=3.51) was supplied by Shanghai Petrochemical (China). Isoprene rubber (IR,2200) was sourced from Rion (Japan). Ethylene propylene rubber (EPR, J-0050, ethylene mass fraction is about 51.6%, M_w=27.20×10^4, M_w/M_n=2.13) was supplied by Jilin Petrochemical (China). High-density polyethylene (HDPE,5000S, MFR: 0.9 g per 10 min, M_w=12.0×10^4, M_w/M_n=4.89) was purchased from Daqing Petrochemical (China).

Sample Preparation

All the blends discussed in this paper were prepared using a Haake torque rheometer (Poly Lab QC, Thermoelectric Co., Ltd, USA). First, composite rubber (EPR and IR) was prepared *via* melt-mixing EPR and IR at a 1:1 mass ratio in a Haake rheometer at 170 °C and 80 r/min for 10 min. Subsequently, PP was mixed with pre-weighed components, including composite rubber and HDPE, at 190 °C and 80 r/min for 15 min, with 2 wt% addition of antioxidant 1010 during processing. Each blend was labeled *x*PP/*u*HDPE@*y*EPR/*z*IR, where *x*, *y*, and *z* correspond to the mass fractions of PP, EPR, and IR, respectively, with the total rubber content $y + z$ fixed at 30. *u* indicates the mass ratio of HDPE to the total mass of the PP/EPR/IR matrix, that is, the amount of HDPE added, expressed in phr. All the composite compositions discussed in this paper were named according to this rule.

Standard specimens for mechanical property testing were produced using a BP-8180-A injection molding machine from China Baopin Precision Instrument Co., Ltd. The injection temperature was set at 200 °C, the injection pressure was 10 MPa, and the holding time was 15 s.

Characterization

Notched Charpy impact testing was performed using a Charpy impact testing machine (XJJUD-5.5(5)) in accordance with ISO 179-1:2000, produced by Xiamen Chongda Intelligent Technology Co., LTD, China. Prior to testing, specimens featuring a 45° V-notch were conditioned at the specified temperature for 12 h, and the results represent the average of five samples.

Tensile strength was evaluated using a computer-controlled universal testing machine (Model5969, INSTRON, USA) following GB/T 1040.2-2006. The dumbbell-shaped specimens were stretched at room temperature with a speed of 50 mm/min. Each test was repeated at least five times, and the average value was taken as the final result.

Dynamic mechanical analysis (DMA) was performed using a DMA 242E analyzer (NETZSCH, Germany) using the single cantilever mode. Temperature scans were conducted from −100 °C to 100 °C at a heating rate of 3 °C/min, using a frequency of 1 Hz and an oscillation amplitude of 30 μm.

The coefficient of thermal expansion (α) of the composites was determined using thermomechanical analysis (TMA) mode of the DMA 242E analyzer with a load of 5 mN and a heating rate of 3 °C /min. The average value of α from −40 °C to 80 °C was calculated.

The broken surface of the sample was examined using a ZEISS Gemini 300 scanning electron microscope (SEM), manufactured in Germany. Prior to the testing, the specimens were cryogenically fractured in liquid nitrogen. Subsequently, the fractured surfaces were etched in *n*-octane at 50 °C for 4 h to remove the rubber phase, and then dried in a vacuum oven at 60 °C for 12 h.

The dispersed-phase structure was further characterized using transmission electron microscopy (TEM). Ultrathin sections, approximately 60 nm in thickness, were obtained using

an EM UC7 ultramicrotome (Leica Microsystems, Japan) at –100 °C. After staining with RuO_4, the slices were analyzed by transmission electron microscopy (JEM-1230, JEOL, Japan) at an acceleration voltage of 200 kV.

The thermal behavior of all samples was characterized using a differential scanning calorimeter (DSC204, NETZSCH, Germany) under a nitrogen atmosphere. Initially, the sample (5–10 mg) was cooled to 0 °C. A melting curve was then obtained by heating the sample to 200 °C at 10 °C/min.

The viscosities of the samples were determined using a rotational rheometer (ARES, TA Instruments, USA). The frequency sweep was performed from 100 rad/s to 0.01 rad/s at 190 °C with a strain amplitude of 5%, ensuring that the measurements were taken within the linear viscoelastic region.

The contact angles between the polymer components and the two test liquids were determined using a DSA 100 droplet shape analyzer (KRUSS, Germany), and the surface tension was calculated according to the Owens-Wendt-Rabel-Kaelble (OWRK) method (the corresponding calculation processes are presented in ESI).[39,40] Distilled water and diiodomethane were employed as polar and nonpolar test liquids, respectively, with a droplet volume of 4 μL.

RESULTS AND DISCUSSION

HDPE@EPR Core-Shell Formation Reduces IR Domain Size for Balanced Stiffness-Toughness in Polypropylene

Fig. 1 presents the SEM images of the PP blends after etching the rubber phase with *n*-octane. The dispersed rubber phase was uniformly distributed in the PP/EPR, PP/IR, and PP/EPR/IR systems. Notably, the interparticle distance (*l*) of the rubber domain in the PP/EPR/IR system was significantly reduced compared to those of the PP/EPR and PP/IR blends. According to Wu's theory,[41] the interparticle distance of rubber particles governs the brittle-ductile transition of polymers, where a smaller interparticle spacing contributes to enhanced toughness. Upon the incorporation of 10 phr HDPE, a typical core-shell structure was formed (Figs. 1d and 1e), which effectively increased the equivalent rubber content.[6] Furthermore, a further reduction in the interparticle distance was observed, accompanied by a broadening of the size distribution of the rubber-dispersed phase.

The irregular porous structure observed by SEM, resulting from the removal of the rubber phase in the PP blends *via n*-octane etching, fundamentally limits the precision of this characterization technique. Therefore, TEM was employed for a more precise analysis of the structural characteristics of the dispersed phase, as illustrated in Fig. 2. The IR phase appears as black spherical domains within the PP matrix, with this contrast arising from the RuO_4 staining treatment, while the gray spherical particles, which exhibit distinct contrast against the matrix, are identified as the EPR phase. In Fig. 2(c), the bright white region encapsulated by the EPR phase is assigned to the HDPE phase. Thus, the four-phase structures comprising PP, IR, EPR, and HDPE can be distinctly distinguished. The particle diameters and their distributions are shown in Fig. 2(d) and Fig. S1 (in the electronic supplementary information, ESI), respectively. In the PP/EPR/IR ternary system, most of the EPR and IR dispersed phases exhibited independent distributions, with the size of the IR (about 590 nm) being significantly larger than that of the EPR (about 360 nm). This phenomenon is consistent with previous literature[36] and can be explained by the higher compatibility between PP and EPR than that between PP and IR. After the introduction of HDPE, a typical core-shell structure with HDPE as the core and EPR as the shell (HDPE@EPR) was clearly observed in the quaternary blend system (see the enlarged region in Fig. 2c), while the IR remained an independent dispersed phase. This structural difference arises from the regulation of interfacial tension according to the spreading coefficient theory;[42] EPR tends to migrate toward the HDPE interface, forming an encapsulating structure.[43,44] To further illustrate the stable core-shell structure formed by HDPE@EPR, the coefficient of thermal expansion (α) of the composites was measured, and the results are presented in Table S1 (in

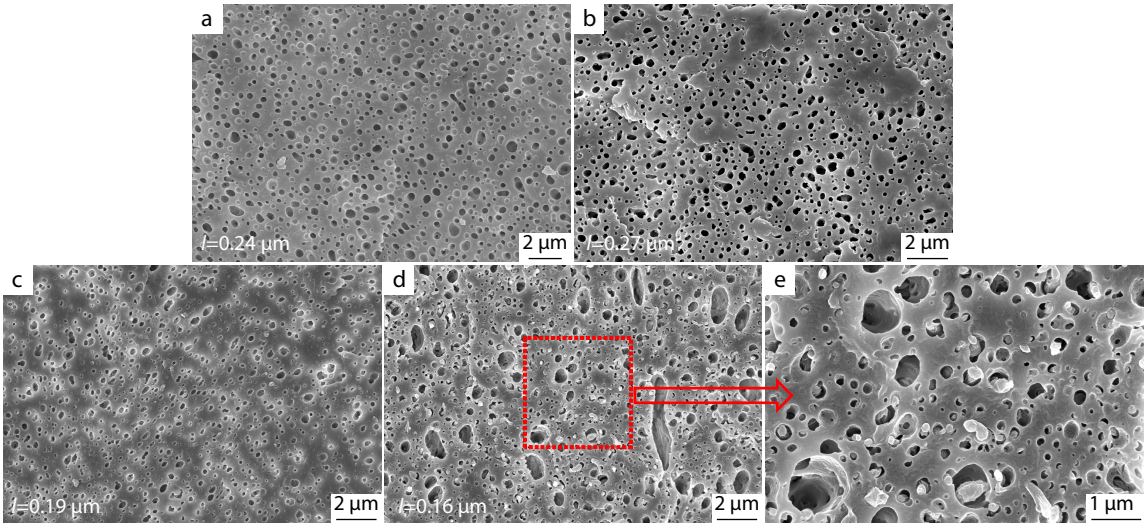

Fig. 1 SEM images of different rubber-toughened or core-shell polypropylene alloys, observed on fracture sections after liquid nitrogen quenching and octane etching: (a) PP/EPR (70/30); (b) PP/IR (70/30); (c) PP/EPR/IR (70/15/15); (d) PP/HDPE@EPR/IR (70/10@15/15); (e) the magnified view of the region marked in (d).

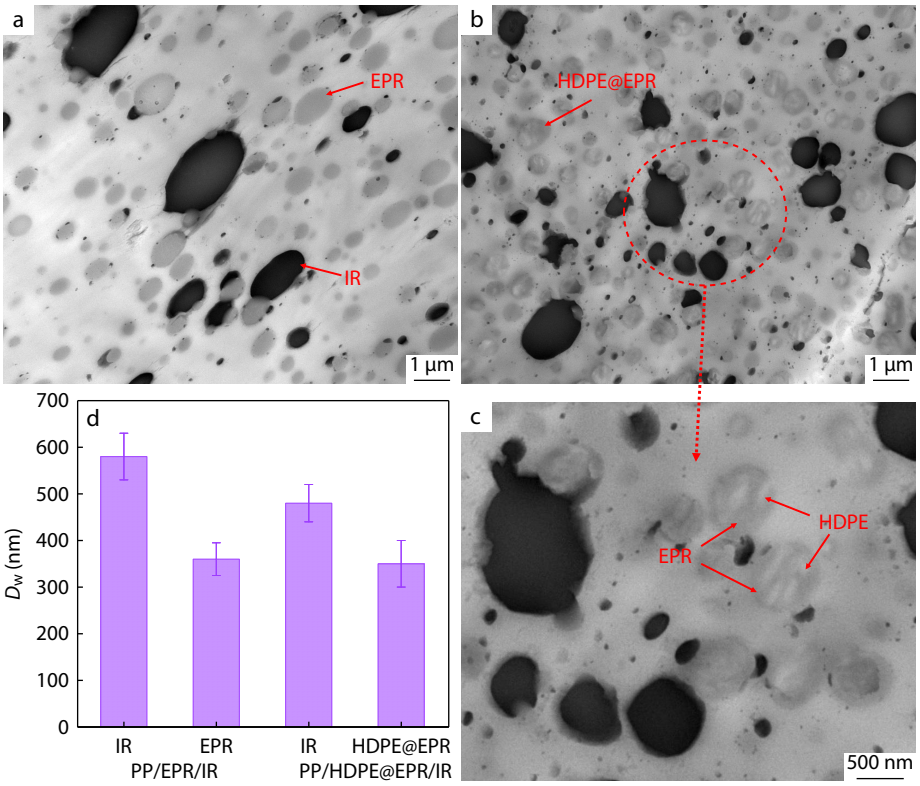

Fig. 2 TEM images of polypropylene alloys toughened with compound rubber/core-shell particles, following RuO_4 staining for contrast enhancement: (a) PP/EPR/IR(70/15/15); (b) PP/HDPE@EPR/IR(70/10@15/15); (c) The magnified view of the region marked in (b). (d) Phase size statistical results for PPR /HDPE/rubber composites.

Table 1 Surface tension results of different components at 25 and 190 °C, respectively.

Sample	Surface tension at 25 °C (mN/m)			Surface tension at 190 °C (mN/m)		
	γ	γ^D	γ^P	γ	γ^D	γ^P
PP	23.64	22.80	0.84	19.90	19.19	0.71
EPR	26.23	25.83	0.40	22.07	21.74	0.33
IR	29.03	27.46	1.57	24.43	23.11	1.32
HDPE	23.86	23.80	0.06	20.08	20.03	0.05

ESI). The a values of HDPE and EPR closely matched those of the PP matrix, which ensured the formation of a stable core-shell structure. Additionally, compared with the PP/EPR/IR system, the size of the IR domain in the quaternary system decreased noticeably. In contrast, although the size of the HDPE@EPR domains remained largely unchanged, there was a significant increase in the number of HDPE@EPR regions dispersed within the matrix. Interfacial tension data and diffusivity calculations for the PP/HDPE, PP/IR, and EPR/IR systems (Tables 1 and 2) suggest that, driven by interfacial tension, EPR and IR tend to form stacked microstructures within the PP matrix.[45] Consequently, IR tends to be anchored near the interface by the EPR phase (Fig. 3). This anchored state restricts IR aggregation. It should be noted that interfacial tension serves as the initial driving force for the evolution of the dispersed phase structure; however, the final morphology of the blend is also influenced by multiple factors, including the viscosities of both the matrix and dispersed phase. Additionally, consistent with the SEM observations, the spacing between the rubber phase particles is considerably reduced, which is attributed to the fine-sized IR domains within the matrix.

Table 2 Spreading coefficients between different components at 190 °C.

Blends system	Spreading coefficient		
	$\lambda_{EPR/IR}$	$\lambda_{IR/EPR}$	$\lambda_{PP/EPR}$ or $\lambda_{PP/IR}$
PP/EPR/IR	−0.37	−0.87	−0.21

Fig. 4(a) illustrates the dynamic mechanical properties of the PP/rubber blends and the PP/rubber/HDPE composites. Two distinct transition peaks were observed in the DMA curves of all samples. The peak in the low-temperature region (from −60 °C to −50 °C) corresponds to the glass transition of the rubber phase, whereas the peak in the higher temperature region (0–30 °C) is attributed to the β-relaxation temperature of PP matrix. It can be observed that the glass transition temperature (T_g) of the composite rubber phase in the PP/EPR/IR and PP/HDPE@EPR/IR systems lies between those of PP/EPR (−63.4 °C) and PP/IR (−54.2 °C). Notably, com-

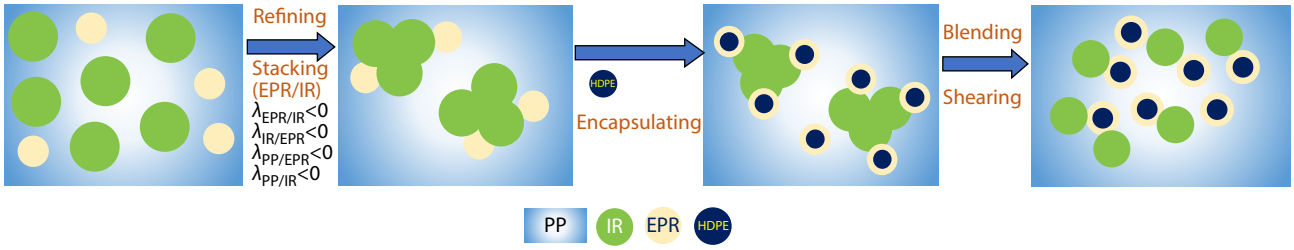

Fig. 3 Schematic of the phase morphology evolution before and after the formation of the HDPE@EPR core-shell structure.

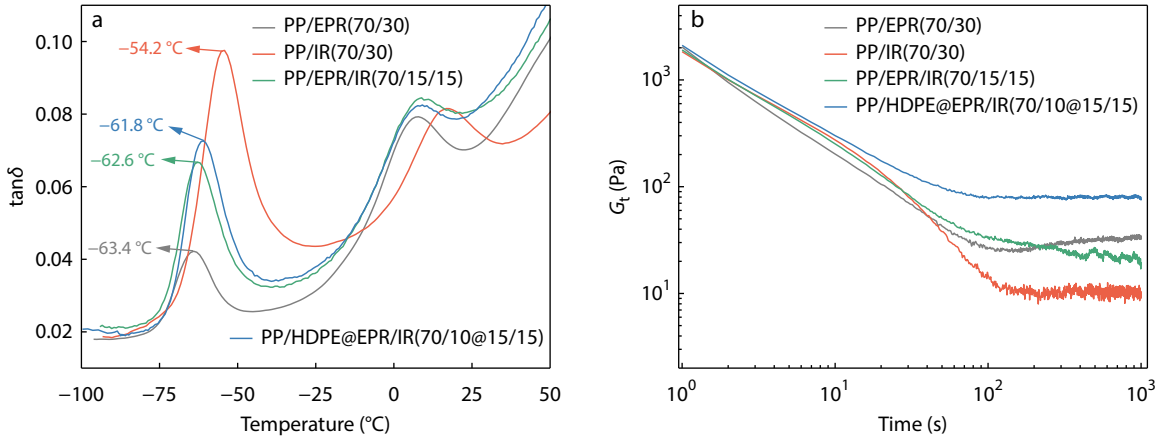

Fig. 4 The performance of PP/rubber blends and PP/rubber/HDPE composites. (a) DMA curves and (b) stress relaxation behaviors of different samples at 190 °C.

pared to the PP/EPR/IR system, the T_g of the composite rubber phase in the PP/HDPE@EPR/IR system shifted slightly toward higher temperatures. This shift may be attributed to the presence of the HDPE core phase. Because the EPR shell shrinks faster than the HDPE core,[5,6,46] the HDPE core exerts an outward pushing force on the EPR shell, partially offsetting the tension at the PP/EPR interface and thereby reducing the free volume of the EPR phase. The resulting compressive stress further decreases the free volume of the EPR, leading to a corresponding increase in T_g.

In the stress relaxation tests, all the PP blends containing 30% rubber exhibited a pronounced long-term relaxation plateau (Fig. 4b). This phenomenon is consistent with previous reports,[8] which indicate that such long-term relaxation behavior primarily originates from the relaxation processes at the interface between the dispersed phase and matrix.[8,47,48] Compared to the PP/EPR, PP/IR, and PP/EPR/IR systems, the PP/HDPE@EPR/IR system shows a significantly higher modulus in the long-term relaxation plateau. Related studies[8,49] suggest that the size and interparticle spacing of rubber-dispersed phase particles are closely related to the stress relaxation behavior. A smaller interparticle spacing promotes the formation of a more developed particle percolation network structure,[49–51] thereby leading to reinforced long-term relaxation behavior. As shown in Fig. 2(d), the development of the HDPE@EPR core-shell structure optimizes the interface and reduces the interparticle spacing, resulting in a stronger particle skeleton network and, consequently, a higher relaxation plateau modulus.

Fig. 5 shows the impact strength of the PP/rubber blends and PP/rubber/HDPE composites at different temperatures, as well as the tensile strength and Young's modulus measured at room temperature. It was demonstrated that single-rubber systems (EPR or IR) endowed limited low-temperature toughening, with EPR outperforming IR owing to its superior PP compatibility. Although the EPR/IR composite rubber blend, where TEM confirmed the isolated dispersion of both particles in the PP matrix (Fig. 2a), yielded marginally higher impact strength than single-rubber systems through T_g-difference synergy, its low-temperature performance remained inadequate. Strikingly, introducing HDPE to construct core-shell HDPE@EPR particles (verified by TEM in Fig. 2b) dramatically enhanced toughness, particularly at −20 °C the PP/HDPE@EPR/IR composite achieved 28.8 kJ/m^2 impact strength, surpassing single-rubber and EPR/IR blends. As shown in Fig. 5(b), the brittle-to-ductile transition temperature (T_{bd}) was significantly reduced from approximately −10 °C for PP/EPR and PP/IR blends to −40 °C for the PP/HDPE@EPR/IR composite. The exceptional toughness is attributed to the reduced interparticle spacing and a strong rubber network enabled by finely dispersed IR during HDPE@EPR core-shell formation, promoting efficient energy dissipation. Notably, compared to pure PP, both the tensile strength and Young's modulus of the PP/rubber and PP/Rubber/HDPE blends decreased to a certain extent owing to the incorporation of the soft rubber phase. Crucially, at a comparable rubber content, this improvement in low-temperature toughness occurred without further sacrificing rigidity: the tensile strength decreased marginally while Young's modulus only decreased by 8% compared to PP/EPR (Fig. 5c). This balance originates from the rigid HDPE core mitigating stiffness loss, whereas the EPR shell couples with finely dispersed IR parti-

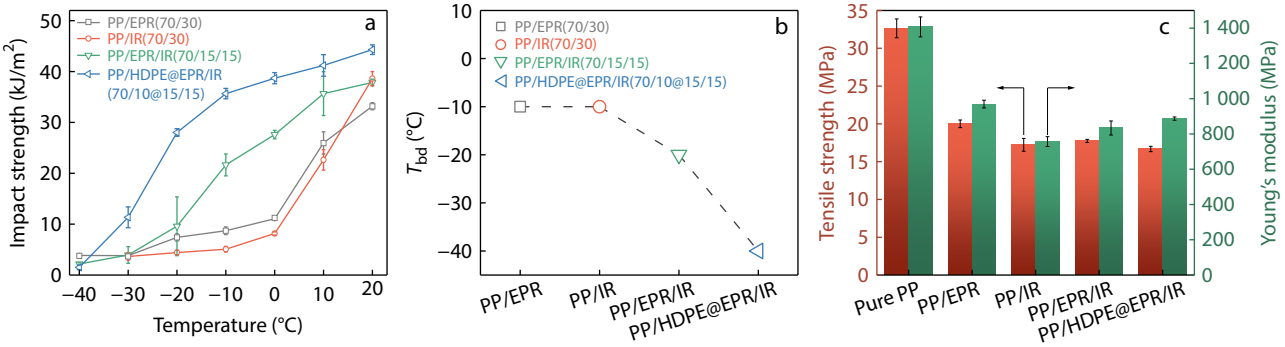

Fig. 5 (a) Impact strength of PP/rubber blends and PP/rubber/HDPE composites at different temperatures; (b) Brittle-to-ductile transition temperature; (c) The tensile strength and Young's modulus of pure PP, PP/rubber blends and PP/rubber/HDPE composites at room temperature.

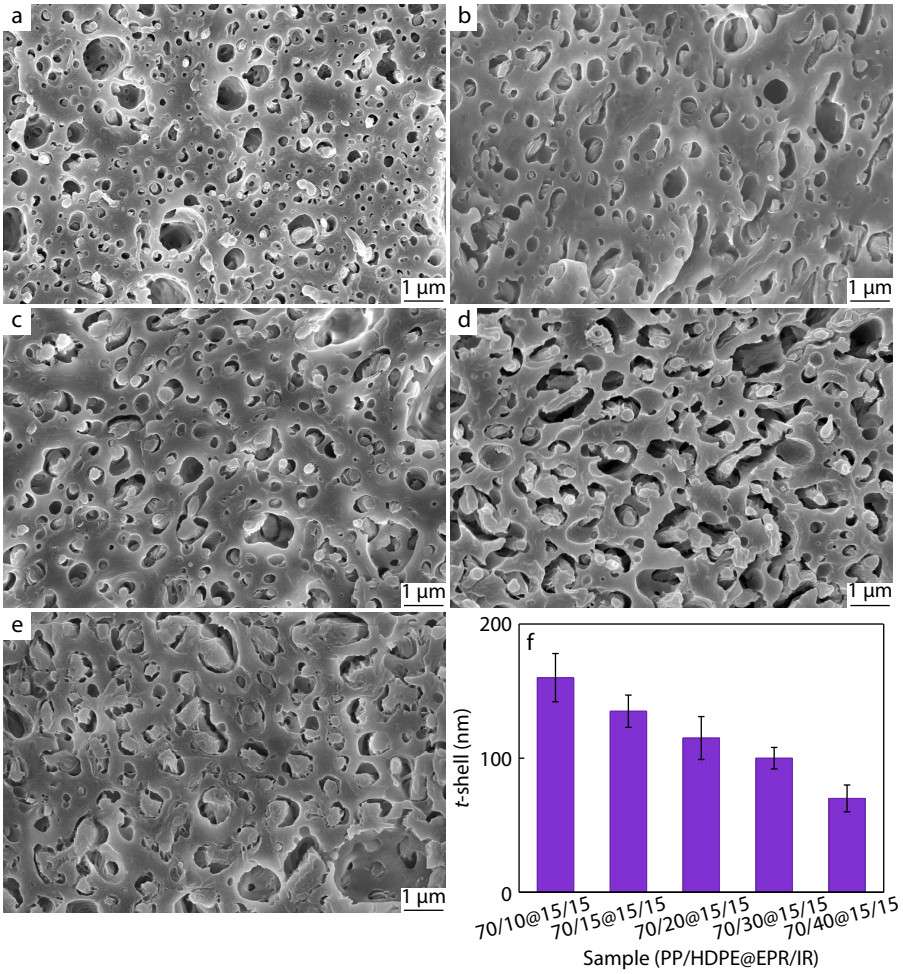

Fig. 6 SEM images of PP/HDPE@EPR/IR blends at different ratios, observed on fracture sections after liquid nitrogen quenching and octane etching: (a) 70/10@15/15; (b) 70/15@15/15; (c) 70/20@15/15; (d) 70/30@15/15; (e) 70/40@15/15. (f) EPR shell thickness.

cles to establish a hierarchical energy dissipation.

Effect of HDPE Core Content on the Toughness of PP/HDPE@EPR/IR Blends

Fig. 6 shows SEM images of PP blends with varying HDPE contents after etching the rubber component with *n*-octane. As the HDPE content increased, a significant reduction in the number of rubber dispersed phases that did not form a core-shell encapsulation structure is observed. Concurrently, the HDPE core phase gradually expanded, whereas the inter-particle spacing of the rubber phase decreased significantly. In addition, the thickness of the EPR shell continued to decrease. At an HDPE loading of 40 phr, the EPR shell thickness decreased below 100 nm. Notably, under these conditions, coalescence occurred among the core-shell structures, as shown in Fig. 6(d), where some HDPE cores were not fully encapsulated by the EPR shell and made direct contact with the surrounding PP matrix.

TEM further revealed the phase structural characteristics of

https://doi.org/10.1007/s10118-026-3771-x

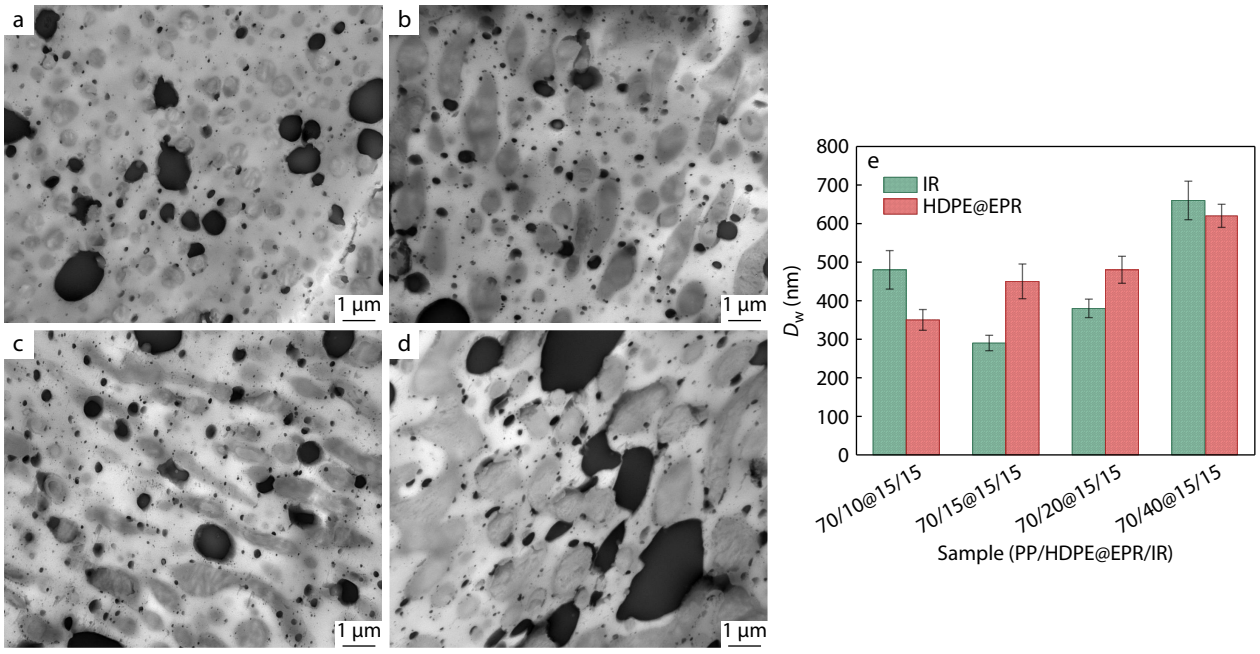

Fig. 7 TEM images of PP/HDPE@EPR/IR blends at different ratios, following RuO4 staining for contrast enhancement: (a) 70/10@15/15; (b) 70/15@15/15; (c) 70/20@15/15; (d) 70/40@15/15. (e) Phase size statistical results for PP/HDPE@EPR/IR samples.

the PP/HDPE@EPR/IR blend, as shown in Fig. 7, with particle diameters distributions illustrated in Fig. S2 (in ESI). TEM analysis indicated that when the HDPE content was 15 phr, the size of the IR phase domains decreased significantly compared to that at 10 phr. However, as the HDPE content increased to 20 phr, the EPR shell thinned and was no longer able to fully encapsulate the HDPE core, consistent with the SEM observations, while the size of the IR phase increased noticeably. The phase evolution process of the PP/HDPE@EPR/IR blend can be explained using the component spreading coefficient theory. Based on the interfacial tension data (Tables 1 and 3), calculations based on the component diffusion coefficient theory indicate that the HDPE and IR phases exhibit a tendency to separate from each other and remain isolated. Specifically, the exposed HDPE phase creates an interfacial repulsion field, which drives the IR phase to detach from its original anchoring sites and migrate toward the EPR-rich regions, leading to aggregation. This migration process reduces the overall interfacial energy of the system, thereby inducing the aggregation of the IR phase. A schematic of the corresponding phase evolution process is shown in Fig. 8.

Fig. 9(a) presents the DMA results for different samples. In the quaternary blend system, two characteristic damping peaks were observed, corresponding to the glass transition of the rubber phase and the relaxation peak of PP. As the HDPE content increases, the relaxation temperature of PP remains essentially unchanged, while the T_g of the rubber phase gradually rises from –61.8 °C to –58.9 °C, further confirming the restrictive effect of the HDPE core on the molecular chain mobility of the EPR rubber. Figs. 9(b) and 9(c) illustrate the dependence of the dynamic modulus on the frequency and stress relaxation behavior of the PP/HDPE@EPR/IR quaternary blends with varying HDPE contents. As shown in Fig. 9(b), the storage modulus in the low frequency region and long-term relaxation plateaus initially increase with the HDPE content and subsequently decrease. As the HDPE content increased, the size of the core-shell particles increased, and the interfacial area expanded, which enhanced the contribution to the long-term relaxation behavior of the system, subsequently increasing the low-frequency storage modulus and stress relaxation plateau modulus. However, when excess HDPE is added, the core-shell structure is disrupted, leading to an increase in the size of the dispersed phase particles and a reduction in the interfacial area. This change results in a corresponding reduction in the plateau modulus.

Fig. 9(d) displays the DSC curves of the system. With increasing HDPE content, the melting point of the HDPE crystalline phase gradually shifted toward higher temperatures. This is primarily attributed to the weakened dilution effect of the EPR phase.[52] Generally, when the crystallization rate is sufficiently low, the crystallizing component can progressively exclude heterogeneous molecular chains from the crystalline regions, forming more perfect spherulites.[5,53–55] As the HDPE content gradually increases, the relative EPR content decreases, allowing HDPE to more effectively exclude EPR molecules, thereby increasing the crystal perfection.

Fig. 10(a) illustrates the variation in impact strength with temperature for PP/HDPE@EPR/IR blends with different HDPE contents. The study found that adjusting the HDPE content to modify the core-shell ratio further optimized the low-temperature toughness of the material. Within the tested temperature range, the impact strength of PP/HDPE@EPR/IR initially

Table 3 Spreading coefficients between different components at 190 °C.

Blends system	Spreading coefficient		
	$\lambda_{IR/HDPE}$	$\lambda_{HDPE/IR}$	$\lambda_{PP/IR}$ or $\lambda_{PP/HDPE}$
PP/IR/HDPE	−1.36	−1.43	0.26

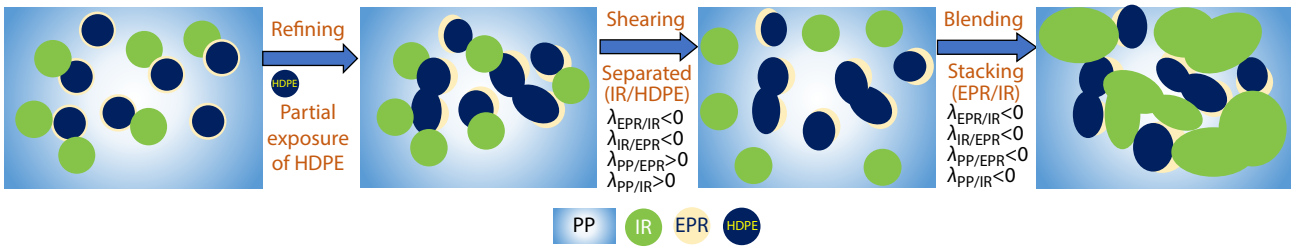

Fig. 8 Schematic illustrating the evolution of phase morphology after the disruption of the HDPE@EPR core-shell structure.

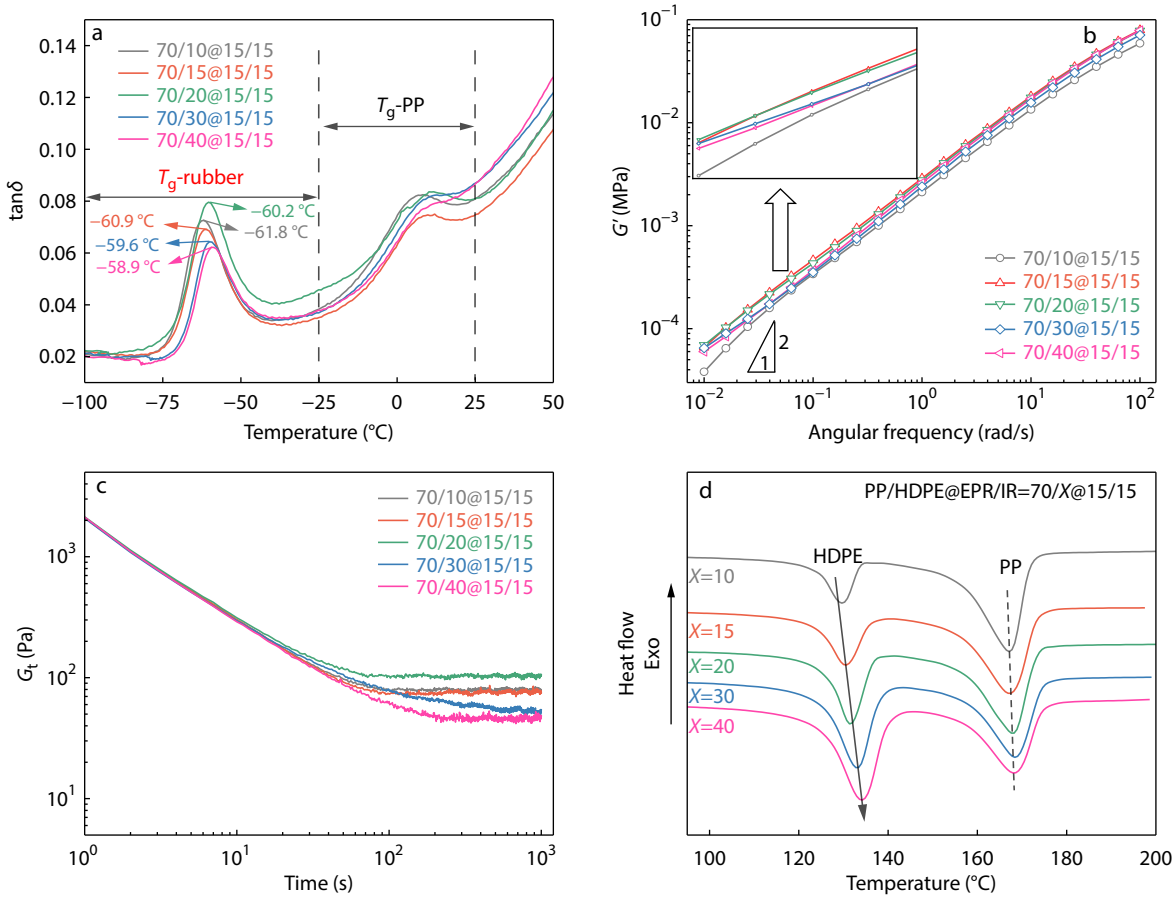

Fig. 9 (a) Dynamic mechanical properties of PP/HDPE@EPR/IR blends; (b) Frequency (ω) dependence of dynamic modulus (G'); (c) Stress relaxation behaviors of different samples at190 °C; (d) DSC melting curves of PP/HDPE@EPR/IR blends, where X denotes the phr of HDPE.

increased and then decreased with increasing HDPE content. Notably, at an HDPE content of 15 phr, where the mass ratio of EPR to HDPE was 1:1, the blend achieved a maximum impact strength of 35.8 kJ/m^2 at –20 °C, demonstrating optimal low-temperature toughness, consistent with the findings reported by Jiang *et al.*[56] To further elucidate the influence of IR rubber size on the low-temperature toughness of PP/HDPE@EPR/IR blends, the dependence of impact strength on IR particle size was investigated, as shown in Fig. 10(b). The impact strength of the PP/HDPE@EPR/IR blend increased significantly with a decrease in the IR rubber particle size. The optimal toughness was achieved when the IR particle size was minimized to 290 nm. This optimum toughness at 15 phr is also directly linked to the well-developed core-shell structure, where the EPR shell is sufficient to maintain the integrity of the dispersed phase, while minimizing the size of the IR phase domains. Conversely, when the HDPE content exceeded 15 phr, the T_{bd} of the material shifts from –40 °C to –30 °C. This deterioration was attributed to the enlarged core size of the core-shell particles, which resulted in a concomitant reduction in the shell thickness. When the shell thickness drops below a critical threshold, it becomes insufficient to induce essential toughening mechanisms such as cavitation or shear yielding. Consequently, the particles lost their efficacy as stress concentrators and failed to initiate crazing or shear bands, ultimately causing the composite to exhibit brittle fracture characteristics. This phenomenon is also supported by the studies of Zheng *et al.*[5] and Jérôme *et al.*[57] Additionally, an excessively high HDPE content also results in a decrease in the actual content of the rubber component. As

https://doi.org/10.1007/s10118-026-3771-x

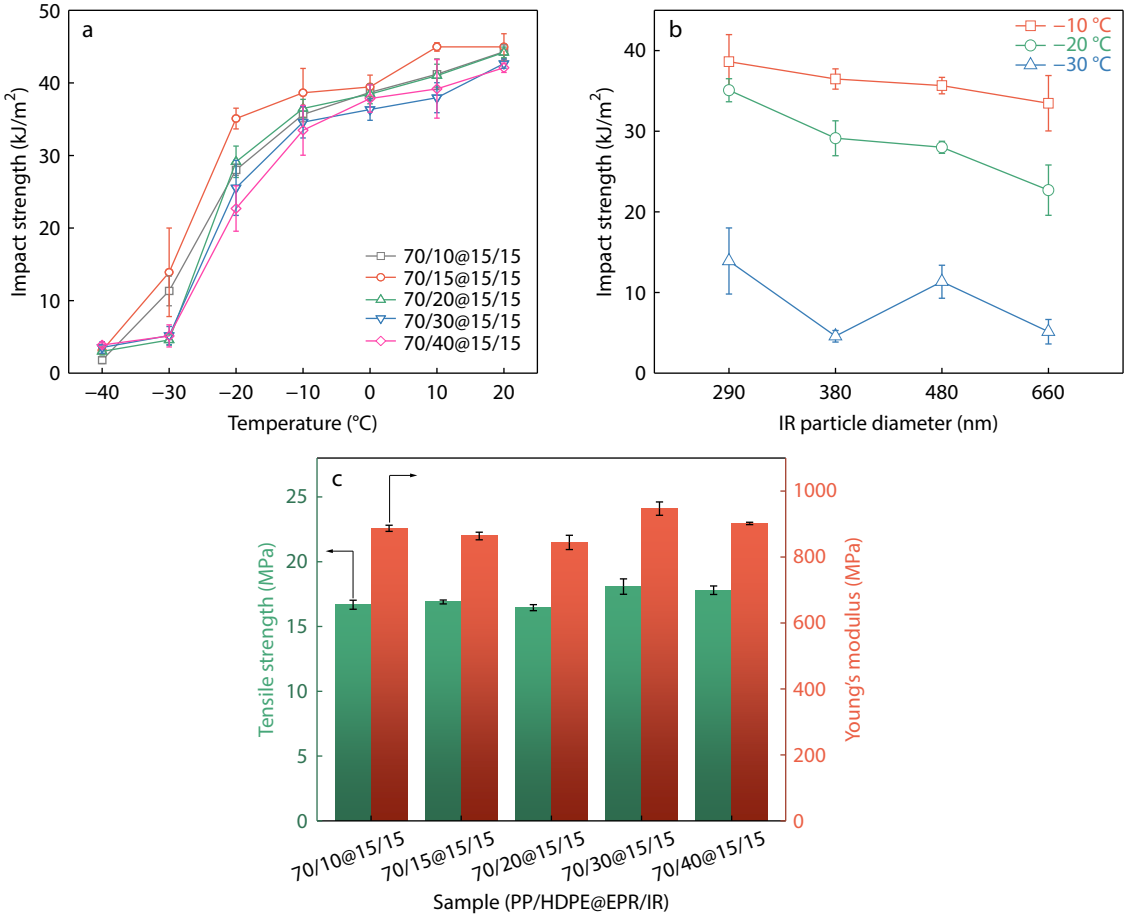

Fig. 10 (a) Impact strength of PP/HDPE@EPR/IR blends at different temperatures; (b) The dependence of low-temperature impact strength on IR particle diameter for PP/HDPE@EPR/IR blends; (c) The tensile strength and Young's modulus at room temperature of PP/HDPE@EPR/IR blends.

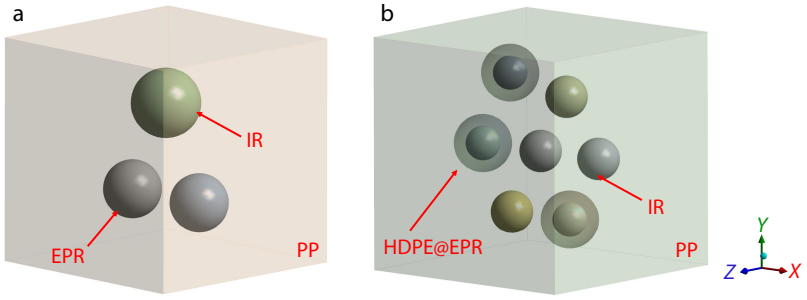

Fig. 11 Schematic diagram of the finite element simulation model of (a) PP/EPR/IR blends and (b) PP/HDPE@EPR/IR blends.

shown in Fig. 10(c), the tensile strength and Young's modulus of the blends increased slightly with increasing HDPE content.

Synergistic Toughening Mechanism of HDPE@EPR and IR Composite Rubber Particles

The theoretical model analysis is based on the following assumptions: (1) the dispersed-phase particles can be approximated as spherical, (2) the interactions between adjacent particles are negligible, (3) a complete core-shell structure is formed between EPR and HDPE, and (4) the material deforms within the elastic range, with the stress-strain relationship following Hooke's law. Based on the results from TEM, SEM, and dynamic thermomechanical analysis, and using the volume fraction of the filler particles, the area ratio of the particles within a unit cell was calculated to determine the cell edge length, thereby establishing the corresponding finite element model. This model aims to investigate the influence of HDPE@EPR core-shell particles, IR particles, and EPR particles on the stress distribution in the PP matrix for both the PP/HDPE@EPR/IR and PP/EPR/IR blend systems. Material parameters were set according to the supplier data, whereas morphological parameters were determined based on TEM observations.

Following the above assumptions, a cubic PP unit cell containing a spherical core–shell particle along with EPR and IR particles at its center was modeled with the specific geometric configuration shown in Fig. 11. A longitudinal uniaxial ten-

sile load was applied to the finite element model, and a three-point bending impact model[58] was used to simulate the impact loading, allowing for the analysis of deformation, strain, and stress distribution within the material.

Fig. 12 presents nephograms of the displacement, strain, and stress fields of the particle model under uniaxial tensile loading. The analysis revealed that the stress distribution patterns around different dispersed-phase particles (HDPE@EPR core-shell particles, EPR particles, and IR particles) share similar characteristics (Figs. 12c and 12f), and significant stress concentration occurred at the two-phase interfaces, with the maximum stress primarily localized near the equatorial region of the particles. According to Eshelby's equivalent inclusion theory,[59] the region of maximum stress near the matrix interface is subjected to tensile forces from the particle toward the matrix, whereas the region of minimum stress near the interface experiences compressive forces from the matrix toward the particle. This stress inhomogeneity induces a local stress concentration within the PP matrix, thereby promoting the initiation and propagation of crazes.

Compared to the PP/EPR/IR blend system, in the PP/HDPE@EPR/IR core-shell composite system, the IR particle size was reduced, and the core-shell particles and small IR rubber particles were inter-penetratingly distributed

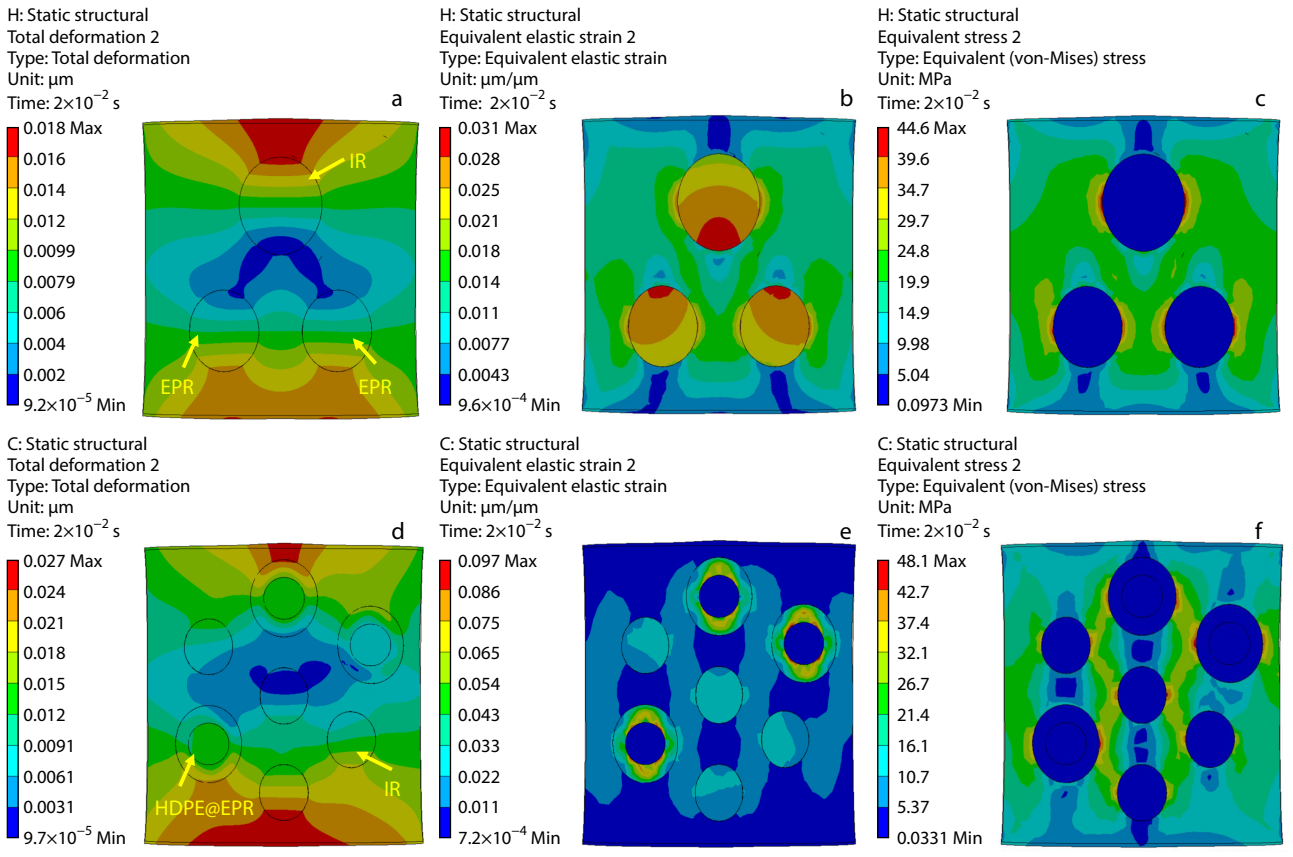

Fig. 12 Finite element simulation of PP/EPR/IR (70/15/15) and PP/HDPE@EPR/IR (70/15@15/15) blends under tensile loading. (a–c) PP/EPR/IR blends; (d–f) PP/HDPE@EPR/IR blends; (a, d) deformation distribution image; (b, e) strain nephogram; (c, f) stress nephogram.

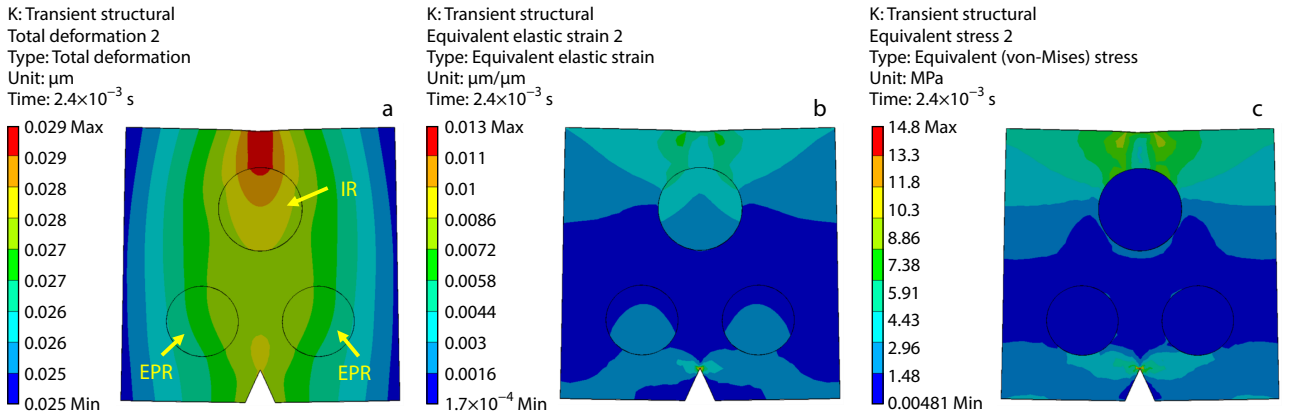

https://doi.org/10.1007/s10118-026-3771-x

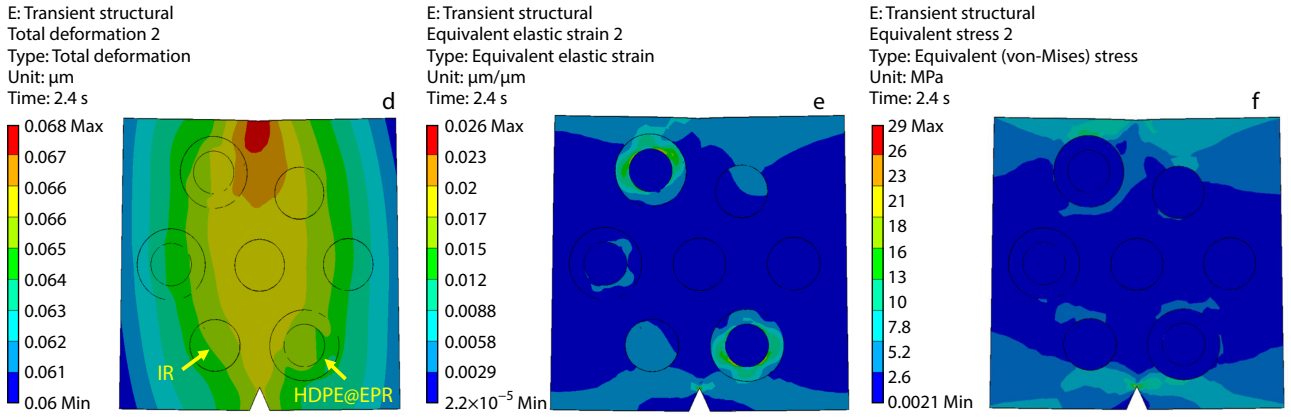

Fig. 13 Finite element simulation of PP/EPR/IR (70/15/15) and PP/HDPE@EPR/IR (70/15@15/15) blends under impact load at room temperature. (a–c) PP/EPR/IR blends; (d–f) PP/HDPE@EPR/IR blends; (a, d) deformation distribution image; (b, e) strain nephogram; (c, f) stress nephogram.

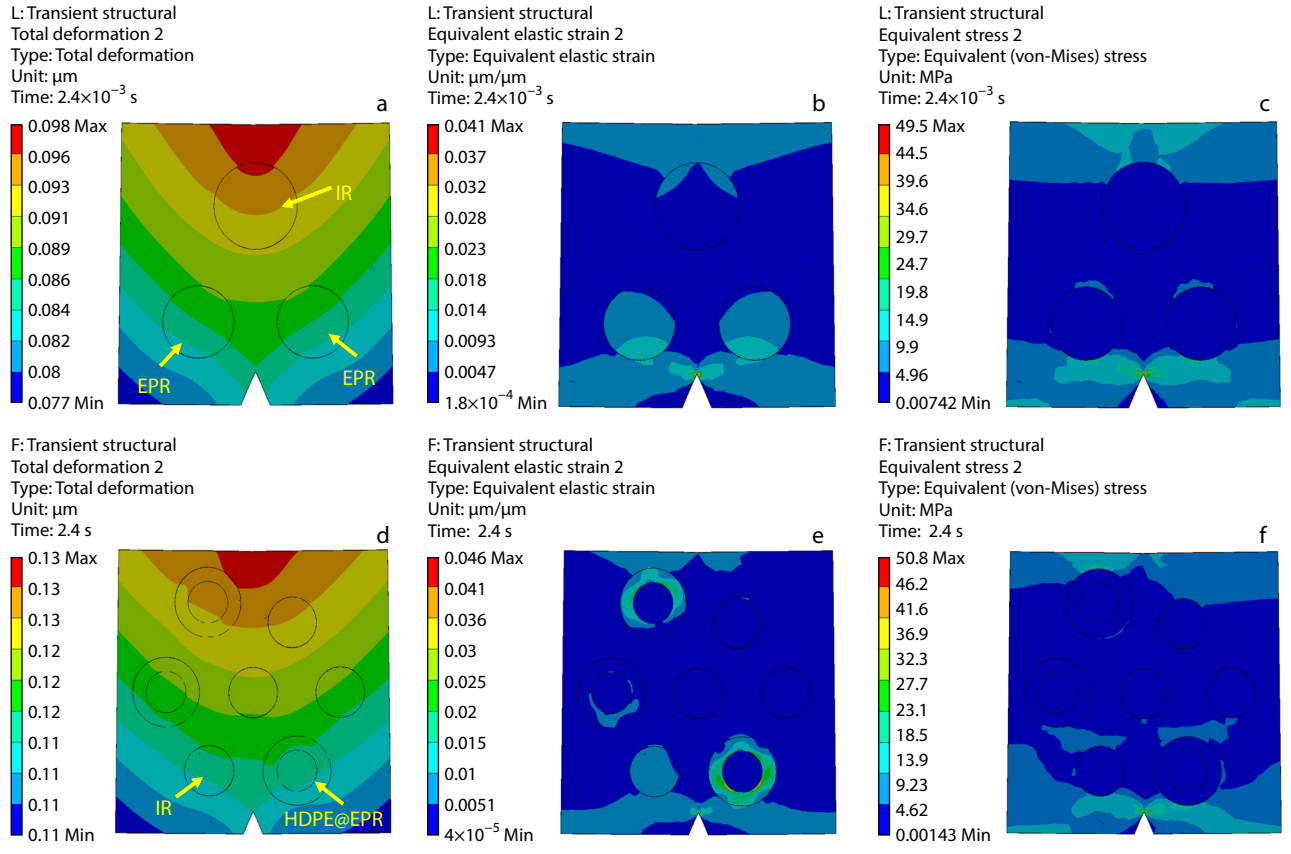

Fig. 14 Finite element simulation of PP/EPR/IR (70/15/15) and PP/HDPE@EPR/IR (70/15@15/15) blends under impact load at low temperature (–20 °C). (a–c) PP/EPR/IR blends; (d–f) PP/HDPE@EPR/IR blends; (a, d) deformation distribution image; (b, e) Strain nephogram; (c, f) Stress nephogram.

throughout the PP matrix. According to percolation theory,[41,60,61] the high-stress zones around the equatorial regions of the core-shell particles and the IR particles are interconnected through the stress field, forming a percolation network.[62] This structure creates a honeycomb-like stress-transfer architecture, demonstrating enhanced stress dispersion capability in tensile simulations. It effectively transmits and redistributes localized high stresses, thereby mitigating the stress concentration phenomena.

Fig. 13 shows the nephograms of the displacement, strain, and stress fields under room-temperature impact loading. A comparison of the finite element simulation results reveals that in the PP/HDPE@EPR/IR blend system, stress is concentrated not only at the particle interfaces (interface effect), but also distributed over a broader region compared to the PP/EPR/IR system. This observation broadens the understanding of energy dissipation mechanisms,[63–65] as it is generally believed that energy dissipation primarily occurs at a single interface. Furthermore, it demonstrates that the synergy between core-shell particles and rubber particles can induce more extensive plastic deformation[66,67] (crazing or shear banding) in the matrix. This significantly enhanced the ener-

gy absorption efficiency of the material at room temperature, thereby effectively improving its impact strength.

Fig. 14 presents nephograms of the deformation, strain, and stress distributions of the blends under low-temperature (–20 ℃) impact loading. Compared to the results at room temperature, the stress and strain distributions at low temperatures are more concentrated. In the PP/EPR/IR system, the stress and strain were primarily localized above the bottom notch and around the EPR particles. Owing to the significant interparticle distance, these stress/strain concentration zones are prone to crack initiation sites. It is worth noting that the large IR particles contribute little to the low-temperature toughness. In contrast, in the PP/HDPE@EPR/IR system, stress and strain are concentrated at the interface of the HDPE@EPR core-shell particles (exhibiting a distinct annular strain distribution), while local stress and strain also appear around the smaller IR particles. The synergy of the core-shell (HDPE@EPR) and small-sized IR rubber particles facilitates a more dispersed stress and strain distribution, thereby suppressing rapid crack propagation within the matrix.[63] Consequently, the toughness of the PP blend was significantly enhanced.

CONCLUSIONS

In summary, the incorporation of HDPE into PP/EPR/IR blends resulted the formation of an HDPE@EPR core-shell structure coupled with finely dispersed IR domains. This minimizes the IR domain size, which creates an extra interface and effectively restricts the mobility of the EPR chains, as evidenced by an increased T_g and a more pronounced long-term relaxation modulus. This structural evolution is governed by the regulation of HDPE content. The optimum HDPE loading of 15 phr yielded the smallest IR rubber particle size (about 300 nm). At this ratio, the PP alloy achieved an impact strength of 35.8 kJ/m^2 at –20 ℃, demonstrating excellent low temperature toughness while maintaining good strength, thereby achieving an optimal balance between strength and toughness. However, a further increase in the HDPE content leads to the aggregation of IR particles. The finite element simulation results demonstrate that in the PP/HDPE@EPR/IR system, a multi-scale percolation network formed between the HDPE@EPR core-shell particles and the IR particles, promoting a uniform stress distribution. Under low temperature impact loading, stress and strain are concentrated around the core-shell interface and the IR particles, which effectively inhibit rapid crack propagation, thereby significantly enhancing the low-temperature toughness of the material. These results confirm a significant synergistic toughening effect between the HDPE@EPR core-shell particles and IR rubber particles. This dual-dispersed phase design strategy offers a promising pathway for the development of high performance PP composites for low-temperature applications.

Conflict of Interests

The authors declare no interest conflict.

Electronic Supplementary Information

Electronic supplementary information (ESI) is available free of charge in the online version of this article at http://doi.org/10.1007/s10118-026-3771-x.

Data Availability Statement

The data that support the findings of this study are available from the corresponding author upon reasonable request.

ACKNOWLEDGMENTS

This work was financially supported by the National Natural Science Foundation of China (No. U22A20151) and the Taiyuan Major Science and Technology Project Fund (2021).

REFERENCES

1 Jia, E. Study on the microstructure adiusting and toughening of polypropylene composites. Thesis, Zhejiang University, **2018**.
2 Chang, E.; Zhao, J.; Zhao, C.; Li, G.; Lee, P. C.; Park, C. B. Scalable production of crosslinked rubber nanofibre networks as highly efficient toughening agent for isotactic polypropylene: toughening mechanism of non-traditional anisotropic rubber inclusion. *Chem. Eng. J* **2022**, *438*, 134060.
3 Ishikawa, M.; Sugimoto, M.; Inoune, T. Mechanism of toughening for polypropylene blended with ethylene–propylene–diene rubber following selective crosslinking. *J. Appl. Polym. Sci.* **1996**, *62*, 1495–1502.
4 Jia, E.; Shangguan, Y.; Xiong, J.; Chen, F.; Zheng, Q. Fabrication of polypropylene blends with excellent low-temperature toughness and balanced toughness-rigidity by a combination of EPR and SEEPS. *J. Appl. Polym. Sci.* **2018**, *135*, 45714.
5 Chen, F.; Shangguan, Y.; Jiang, Y.; Qiu, B.; Luo, G.; Zheng, Q. Toughening with little rigidity loss and mechanism for modified polypropylene by polymer particles with core–shell structure. *Polymer* **2015**, *65*, 81–92.
6 Jia, E.; Zhao, S.; Shangguan, Y.; Zheng, Q. Toughening mechanism of polypropylene bends with polymer particles in core-shell structure: Equivalent rubber content effect related to core-shell interfacial strength. *Polymer* **2019**, *178*, 121602.
7 Qian, Z.; Wang, X.; Qiu, B.; Zhong, J.; Li, X. Analysis of strengthening and toughening mechanism for polypropylene with core shell dispersed phase. *J. Funct. Mater.* **2019**, *50*, 7029–7034.
8 Li, M.; Zhu, L.; Chen, F.; Wu, Q.; Shangguan, Y.; Zheng, Q. Rheology study on polypropylene blends with in situ core-shell dispersed particles. *Acta Polymerica Sinica* (in Chinese) **2022**, *53*, 1399–1408.
9 Zhao, S.; Shangguan, Y.; Wu, Q.; Li, Z.; Zheng, Q. Toughening mechanism of PP/EPR/SiO2 composites with superior low-temperature toughness. *Compos. Sci. Technol.* **2021**, *207*, 108691.
10 Jia, E.; Zhao, S.; Shangguan, Y.; Zheng, Q. A facile fabrication of polypropylene composites with excellent low-temperature toughness through tuning interfacial area between matrix and rubber dispersion by silica nanoparticles located at the interface. *Compos. Sci. Technol.* **2019**, *184*, 107846.
11 Zhang, L.; Li, C.; Huang, R. Toughness mechanism of polypropylene/elastomer/filler composites. *J. Polym. Sci., Part B: Polym. Phys.* **2005**, *43*, 1113–1123.
12 Yang, H.; Zhang, X.; Qu, C.; Li, B.; Zhang, L.; Zhang, Q.; Fu, Q. Largely improved toughness of PP/EPDM blends by adding nano-SiO_2 particles. *Polymer* **2007**, *48*, 860–869.
13 Zhu, L.; Li, M.; Zhao, S.; Bao, S.; Chen, F.; Shangguan, Y.; Wu, Q.;

Graphical Abstract

Synergistic Toughening of Polypropylene Alloys Using Core-Shell High-density Polyethylene/Ethylene-Propylene Rubber and Isoprene Rubber Composite Rubber Particles

Hai-Bo Wang, Ang-Xuan Wu, Jia-Hao Shen, Xiao-Tian Nan, Feng-Bo Zhu, Wen-Wen Yu, and Qiang Zheng

Taiyuan University of Technology; Tsinghua University; Zhejiang University

The low-temperature toughness of polypropylene (PP) composites is improved by a dual-dispersed phase structure, achieved through the interfacial tension-induced refinement of isoprene rubber (IR) phase with high-density polyethylene (HDPE)@ ethylene-propylene rubber (EPR) core-shell particles.

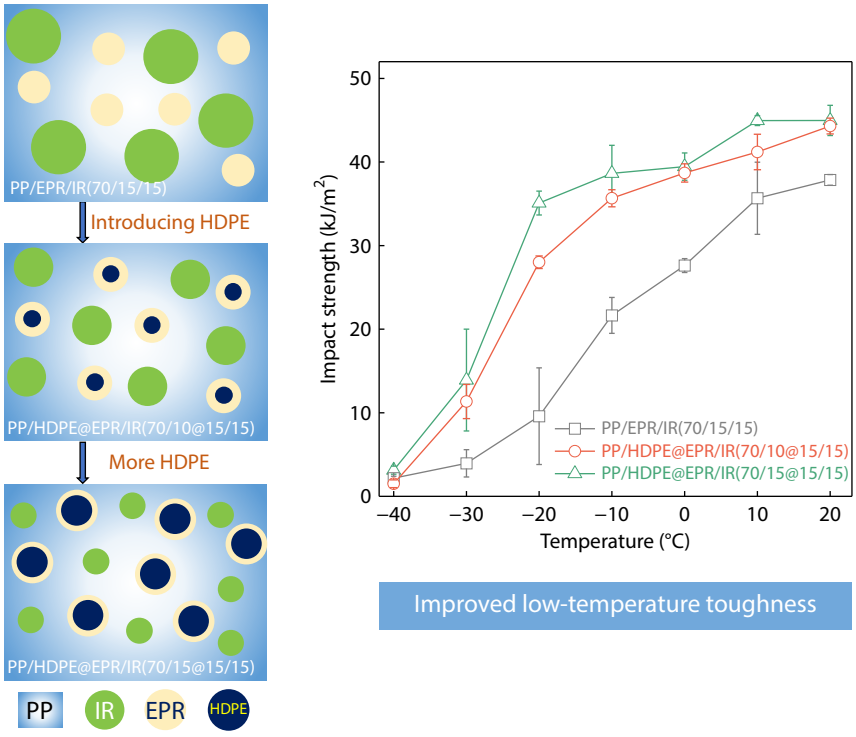

Chinese J. Polym. Sci. 2026 *https://doi.org/10.1007/s10118-026-3771-x*

Zheng, Q. Ultra-high impact PPR composites at low-temperature through enhanced preferential loading of nanoparticles at polymeric interface induced by properly vulcanized rubber dispersed phase. *Compos. Sci. Technol.* **2022**, *227*, 109593.

14 Khodabandelou, M.; Razavi Aghjeh, M. K.; Mazidi, M. M. Fracture toughness and failure mechanisms in un-vulcanized and dynamically vulcanized PP/EPDM/MWCNT blend-nanocomposites. *RSC Adv.* **2015**, *5*, 70817–70831.

15 Sun, Z.; Zhang, Y.; Shao, H.; He, A. In situ reactive compatibilization of polypropylene/trans-1,4-poly(isoprene-co-butadiene) rubber (TBIR) blends with balanced toughness and stiffness *via* dynamic vulcanization. *React. Funct. Polym.* **2019**, *142*, 60–68.

16 Haghnegahdar, M.; Naderi, G.; Ghoreishy, M. H. R. Fracture toughness and deformation mechanism of un-vulcanized and dynamically vulcanized polypropylene/ethylene propylene diene monomer/graphene nanocomposites. *Compos. Sci. Technol.* **2017**, *141*, 83–98.

17 Chen, F. Structure-property relationships of impact polypropylene copolymer and toughening for polypropylene. Thesis, Zhejiang University, **2015**.

18 Zhang, Y. The study on polypropylene modified by thermo-cross-linked rubber. Thesis, Beijing University of Chemical Technology, **2018**.

19 Wang, F.; Drzal, L. T.; Qin, Y.; Huang, Z. Enhancement of fracture toughness, mechanical and thermal properties of rubber/epoxy composites by incorporation of graphene nanoplatelets. *Compos. A* **2016**, *87*, 10–22.

20 Tan, H. Polyolefin materials: structure of impact polypropylene copolymer and properties of conductive composites. Thesis, Zhejiang University, **2006**.

21 Cheng, H. Preparation and properties of synergistic toughening modified polypropylene with β-nucleating agent and nano-silica. Thesis, Zhejiang University, **2021**.

22 Margolina, A.; Wu, S. Percolation model for brittle-tough transition in nylon/rubber blends. *Polymer* **1988**, *29*, 2170–2173.
23 Zhang, C.; Shangguan, Y.; Tan, Y.; Chen, F.; Huang, Z.; Zheng, Q. Rheological behavior of impact polypropylene copolymer and its fractions. *Chem. J. Chin. Univ.* **2012**, *33*, 430.
24 Qiu, B. Controlling of the dispersed phase and structure-property relationship for imapct polypropylene copolymer. Thesis, Zhejiang University, **2014**.
25 Wu, H. The Morphology development of EPDM/PP TPV during dynamic vulcaniztion and its relationship with properties of TPV. Thesis, Beijing University of Chemical Technology, **2016**.
26 Zheng, H.; Zhai, W.; Bao, J.; Zheng, W. Influences of nanosilica on vulcanization behavior and physical foaming behavior of micro-crosslinked EPDM. *J. Funct. Mater.* **2020**, *51*, 6084–6090.
27 Zhang, L. Construction and properties of micro crosslinking structure of PP/modified castor fiber composites. *Plast. Sci. Technol.* **2021**, *49*, 23–27.
28 Bao, W.; Wang, X.; Li, L.; Jin, J.; Pan, Y.; Liang, H.; Ji, X.; Jiang, W. Core-shell structure strategy to prepare super-tough poly(lactic acid) composites with balanced stiffness and toughness. *Polym. Sci. Technol.* **2026**, *2*, 505–514.
29 Beylergil, B.; Ozturkmen, M. B.; Al-Nadhari, A.; Yildiz, S.; Aydoğan, B.; Yildiz, M. Enhancement of mechanical properties of carbon fiber epoxy composites using methylmethacrylate-butadiene-styrene (MBS) core-shell nanoparticles. *J. Compos. Mater.* **2025**, *59*, 1533–1552.
30 Li, F.; Gao, Y.; Zhang, Y.; Jiang, W. Design of high impact thermal plastic polymer composites with balanced toughness and rigidity: Toughening with core-shell rubber modifier. *Polymer* **2020**, *191*, 122237.
31 Tang, Y. H.; Zhang, N.; Bao, W.; Jiang, W.; Lin, Y.; Su, Z. H. Critical role of ethylene-propylene block copolymer in impact polypropylene copolymer. *Chinese J. Polym. Sci.* **2024**, *42*, 344–351.
32 Fowler, M. E.; Keskkula, H.; Paul, D. R. Mechanical behavior of dual-rubber-modified SAN. *J. Appl. Polym. Sci.* **1988**, *35*, 1563–1571.
33 Zhu, L. D.; Yang, H. Y.; Cai, G. D.; Zhou, C.; Wu, G. F.; Zhang, M. Y.; Gao, G. H.; Zhang, H. X. Submicrometer-sized rubber particles as "craze-bridge" for toughening polystyrene/high-impact polystyrene. *J. Appl. Polym. Sci.* **2013**, *129*, 224–229.
34 Rehman, A.; Saeed, F.; Shuib, R. K. Characterisation and properties of polyisoprene (IR)/polybutadiene (BR) rubber blends-reinforced silanised silica nano-filler. *J. Rubber Res.* **2022**, *25*, 223–230.
35 Ciullo, P. A.; Hewitt, N., Compounding materials. in *The rubber formulary*, Ciullo, P. A.; Hewitt, N., Eds. William Andrew Publishing, Norwich, NY, **1999**, pp. 4–49.
36 Bao, S.; Zhu, L.; Wang, H.; Luo, H.; Chen, F.; Yu, W.; Zhang, Z.; Zhuang, X.; Wu, Q.; Shangguan, Y.; Zheng, Q. Synergistic effect of compound rubber and SiO_2 nanoparticles on low-temperature toughening and balanced stiffness-toughness of random copolymer polypropylene nanocomposites. *Compos. Sci. Technol.* **2023**, *242*, 110210.
37 Zhao, S.; Hu, R.; Zhu, L.; Li, M.; Chen, F.; Wu, Q.; Shangguan, Y.; Zheng, Q. Adjustable brittle-ductile transition behavior and rheological behavior of polypropylene random copolymer nanocomposites through well interfacial-loaded nanoparticles. *Compos. B: Eng.* **2022**, *238*, 109939.
38 Jiang, C.; Jiang, B.; Yang, Y.; Huang, Z.; Liao, Z.; Sun, J.; Wang, J.; Yang, Y. Enhanced multiphase interfacial interaction of impact polypropylene copolymer by in-situ introducing polyethylene. *Polymer* **2021**, *214*, 123373.
39 Davis, B. W. Estimation of surface free energies of polymeric materials. *J. Colloid Interface Sci.* **1977**, *59*, 420–428.
40 Kaelble, D. H. Dispersion-polar surface tension properties of organic solids. *J. Adhes.* **1970**, *2*, 66–81.
41 Wu, S. A generalized criterion for rubber toughening: the critical matrix ligament thickness. *J. Appl. Polym. Sci.* **1988**, *35*, 549–561.
42 Hobbs, S. Y.; Dekkers, M. E. J.; Watkins, V. H. Effect of interfacial forces on polymer blend morphologies. *Polymer* **1988**, *29*, 1598–1602.
43 Hemmati, M.; Nazokdast, H.; Shariat Panahi, H. Study on morphology of ternary polymer blends. I. Effects of melt viscosity and interfacial interaction. *J. Appl. Polym. Sci.* **2001**, *82*, 1129–1137.
44 Hemmati, M.; Nazokdast, H.; Shariat Panahi, H. Study on morphology of ternary polymer blends. II. Effect of composition. *J. Appl. Polym. Sci.* **2001**, *82*, 1138–1146.
45 Mao, Z.; Zhang, J. Largely improved the low temperature toughness of acrylonitrile-styrene-acrylate (ASA) resin: fabricated a core-shell structure of two elastomers through the differences of interfacial tensions. *Appl. Surf. Sci.* **2018**, *444*, 345–354.
46 Shangguan, Y.; Chen, F.; Yang, J.; Jia, E.; Zheng, Q. A new approach to fabricate polypropylene alloy with excellent low-temperature toughness and balanced toughness-rigidity through unmatched thermal expansion coefficients between components. *Polymer* **2017**, *112*, 318–324.
47 Graebling, D.; Benkira, A.; Gallot, Y.; Muller, R. Dynamic viscoelastic behaviour of polymer blends in the melt—experimental results for PDMS/POE-DO, PS/PMMA and PS/PEMA blends. *Eur. Polym. J.* **1994**, *30*, 301–308.
48 Svoboda, P.; Kressler, J.; Ougizawa, T.; Inoue, T.; Ozutsumi, K. FTIR and calorimetric analyses of the specific interactions in poly(ε-caprolactone)/poly(styrene-co-acrylonitrile) blends using low molecular weight analogues. *Macromolecules* **1997**, *30*, 1973–1979.
49 Shen, J.; Zhang, Z.; Yu, W.; Wang, J.; Wang, W.; Shangguan, Y.; Zheng, Q. Phase morphology evolution and rheological behavior of toughened polypropylene composite with controllable brittle–ductile transition temperature using SEPS@HDPE core–shell structure. *Engineering* **2025**, *50*, 128–135.
50 Nemirovski, N.; Siegmann, A.; Narkis, M. Morphology of ternary immiscible polymer blends. *J. Macromol. Sci., Part B* **1995**, *34*, 459–475.
51 Lertwimolnun, W.; Vergnes, B. Influence of compatibilizer and processing conditions on the dispersion of nanoclay in a polypropylene matrix. *Polymer* **2005**, *46*, 3462–3471.
52 Zhang, C.; Shangguan, Y.; Chen, R.; Wu, Y.; Chen, F.; Zheng, Q.; Hu, G. Morphology, microstructure and compatibility of impact polypropylene copolymer. *Polymer* **2010**, *51*, 4969–4977.
53 Cheng, D.; Feng, J.; Yi, J. Influence of nucleation on the brittle-ductile transition temperature of impact-resistant polypropylene copolymer: from the sight of phase morphology. *J. Appl. Polym. Sci.* **2012**, *123*, 1784–1792.
54 Tanaka, H.; Nishi, T. Local phase separation at the growth front of a polymer spherulite during crystallization and nonlinear spherulitic growth in a polymer mixture with a phase diagram. *Phys. Rev. A* **1989**, *39*, 783–794.
55 Keith, H. D.; Padden, F. J., Jr. A Phenomenological theory of spherulitic crystallization. *J. Appl. Phys.* **1963**, *34*, 2409–2421.
56 Li, F.; Zhang, N.; Gao, Y.; Yan, N.; Jin, J.; Su, Z.; Jiang, W. In situ formation of core-shell rubber particles in polypropylene matrix by melt blending and its effects on the toughness and stiffness of the composites. *Polym. Eng. Sci.* **2022**, *62*, 4090–4099.
57 Luzinov, I.; Xi, K.; Pagnoulle, C.; Huynh-Ba, G.; Jérôme, R. Composition effect on the core–shell morphology and mechanical properties of ternary polystyrene/styrene–butadiene rubber/polyethylene blends. *Polymer* **1999**, *40*, 2511–2520.
58 Meiqin, L.; Xing, M.; Shuai, L.; Fei, P. In *Data analysis of three-point*

bending deformation based on finite element method, Proc.SPIE, **2024**, p. 132264P.
59 Eshelby, J. D. The determination of the elastic field of an ellipsoidal inclusion, and related problems. *P. Roy. Soc. A-Math. Phy.* **1957**, *241*, 376–396.
60 Wu, S. Chain structure, phase morphology, and toughness relationships in polymers and blends. *Polym. Eng. Sci.* **1990**, *30*, 753–761.
61 Wu, S. Control of intrinsic brittleness and toughness of polymers and blends by chemical structure: a review. *Polym. Int.* **1992**, *29*, 229–247.
62 Du, P.; YU, J.; Lin, P.; Song, Y.; Zheng, Q. Effect of rubber and inorganic rigid particles on fracture behavior of injection-molded PVC nanocomposites. *Acta Polymerica Sinica* (in Chinese) **2011**, 1395–1401.
63 Liang, J. Z.; Li, R. K. Y. Rubber toughening in polypropylene: A review. *J. Appl. Polym. Sci.* **2000**, *77*, 409–417.
64 Kim, H.-J.; Lee, K.-J.; Seo, Y. Enhancement of interfacial adhesion between polypropylene and nylon 6: effect of surface functionalization by low-energy ion-beam irradiation. *Macromolecules* **2002**, *35*, 1267–1275.
65 Mukhopadhyay, S.; Deopura, B.; Alagiruswamy, R. Interface behavior in polypropylene composites. *J. Thermoplast. Compos. Mater.* **2003**, *16*, 479–495.
66 Okubo, K.; Fujii, T.; Thostenson, E. T. Multi-scale hybrid biocomposite: processing and mechanical characterization of bamboo fiber reinforced PLA with microfibrillated cellulose. *Compos. A* **2009**, *40*, 469–475.
67 Şahin, A. E.; Fidan, S.; Çetin, B.; Sınmazçelik, T. Comparison of the usage of nut shell, walnut shell, and pistachio shell as a reinforcement particle on the mechanical and wear performance of polypropylene. *J. Appl. Polym. Sci.* **2024**, *141*, e55248.

https://doi.org/10.1007/s10118-026-3771-x